Bilateral Macro–Micro Teleoperation Using Magnetic Levitation

Moein Mehrtash, *Member, IEEE*, Naoaki Tsuda, and Mir Behrad Khamesee, *Member, IEEE*

***Abstract*—This paper introduces a novel magnetic-haptic micromanipulation platform with promising potential for extensive biological and biomedical applications. The platform has three basic subsystems: a magnetic untethered microrobotic system, a haptic device, and a scaled bilateral teleoperation system. A mathematical force model of the magnetic propulsion mechanism is developed, and used to design PID controllers for magnetic actuation mechanism. A gain-switching position–position teleoperation scheme is employed for this haptic application. In experimental verifications, a human operator controls the motion of the microrobot via a master manipulator for dexterous micromanipulation tasks. The operator can feel force during microdomain tasks if the microrobot encounters a stiff environment. The effect of hard contact is fed back to the operator's hand in a 20 mm $\times$ 20 mm $\times$ 30 mm working envelope of the proposed platform. Conducting several experiments under different conditions, rms of position tracking errors varied from 20 to 40 μm.**

***Index Terms*—Haptic, magnetic levitation, mechatronics, microrobotic, teleoperation.**

I. Introduction

RECENT advancements in micro/nano technology have opened new horizons in biomechatronics. Researchers have incorporated many disciplines to advance biocompatible mechatronic systems for wide microdomain applications, such as cell/scaffold micromanipulation, cell injection, microsurgery, and microdrug delivery. Although intense research has been undertaken on microassembly and micromanipulation of micro parts for MEMS, far too few studies explored the field of biomicromanipulations. The first generation of micromanipulation systems may perhaps concern semiconductor-manufacturing techniques; however, these costly systems have not been well adapted for biomicromanipulation. Numerous research-made micromanipulation prototypes have led to "proof-of-concept" systems in the field of bioengineering, including optical trapping [1], electrokinetics [2]–[4], magnetics [5], and MEMS-based micromanipulation [6]. In comparison with manipulation in the macroworld, the main research in micromanipulations is focused on the following challenges: 1) the design of miniaturized parts of manipulation systems and 2) the scaling effect phenomena [7].

A large and growing body of literature under the subject of micromanipulation has investigated contact-based methods (CBM), a MEMS-based end-effector attached to a high precision macrodomain robot. Generally, these customized stations are advanced to address the grasp-and-release capabilities of MEMS microgrippers [6], [8]–[10]. Perhaps, the most serious drawback of these techniques is that the arms and connections of macrodomain robots constrain the working envelope of end-effectors. Furthermore, as macrodomain robots are not designed to apply microdomain forces, they may destroy manipulated objects. The miniaturization of a mobile robot is one of the more practical and reliable ways of using micromanipulation to remedy the CBM drawbacks. Such a mobile robot consists of miniature actuators, sensors, electronic parts, and power sources. These robots use numerous locomotion techniques such as swimming [11], paddling [12], [13], and flying [14]. Although the literature reports consequential advances in the design and implementation of such microrobotic systems, there is still a considerable challenge for the integration of the on-board miniaturized power supply, which significantly increases the size of microrobots. However, untethered microrobotic systems show promising approaches in accommodating the power supply constraints. These systems use off-board power sources such as electrostatic force [4], [15], photothermal expansion [16], and electromagnetic force [17], [18]. Electrostatic and photothermal methods might not still be suitable for biomicromanipulation as: 1) a high-intensity electric field increases gas bubble formation and also the temperature of workspace, and 2) high optical intensity can cause photodamage of living cells, and increase the temperature of workspace; both situations may damage living cells. Biomicromanipulation using a magnetic field does not cause physical damage to living cells, and the growth rate of living cells is also not affected by a magnetic field [19], [20]. Hence, this study will focus on the potential of magnetic actuation technology for micromanipulations in biological/biomedical applications.

The second challenge in the design of micromanipulation systems is the scaling effect phenomenon that changes the dominance of physical phenomena in microdomain [7]. The insignificant unmodeled forces in the macroworld such as friction and adhesion act as dominant sources of force in the microworld. Therefore, the better these forces are modeled in the design process of microrobotic systems, the more reliable are the micro-object interactions achieved. However, these complicated

Manuscript received July 22, 2010; revised November 17, 2010; accepted February 7, 2011. Date of publication April 5, 2011; date of current version May 6, 2011. Recommended by Guest Editor C. H. Menq. This work was supported in part by the Natural Sciences and Engineering Research Council of Canada and in part by the Canada Foundation for Innovation.

M. Mehrtash and M. B. Khamesee are with the Department of Mechanical and Mechatronics Engineering, University of Waterloo, Waterloo, ON N2 L 3G1, Canada (e-mail: khamesee@uwaterloo.ca).

N. Tsuda is with the Department of Mechanical Engineering, Wakayama National College of Technology, Gobo 644-0023, Japan.

Color versions of one or more of the figures in this paper are available online at http://ieeexplore.ieee.org.

Digital Object Identifier 10.1109/TMECH.2011.2121090

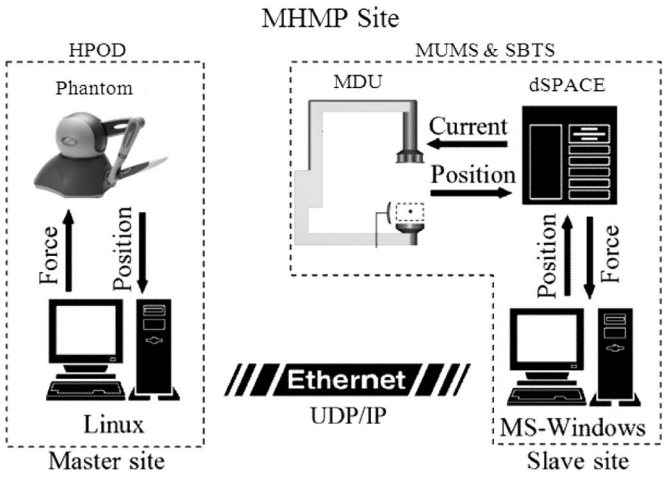

Fig. 1. Schematic of the MHMP.

forces have been poorly observed, so human intervention can significantly enhance the micromanipulation tasks and avoid imperceptible failures. In such a system [21], the "Haptic Loupe" was developed to support micromanipulations by a human operator. Similar haptic micromanipulation systems were proposed for micromanufacturing and microassembly [22]–[24]. In addition, haptic microrobotic systems show a significant promise in biological/biomedical applications that professional human operators perform dexterous micromanipulations, such systems as da vinci telerobotic surgical system in conjunction with tension measuring device [25], haptic-enabled tumor localization system [26], cell injection platforms [4], [27], [28], and cell/scaffold force-feedback manipulator [6]. Therefore, to advance our research-made prototype for biomicromanipulation applications, a "Haptic Loupe" is integrated with our micromanipulation system.

This study introduces a novel magnetic-haptic micromanipulation platform (MHMP) with promising potential for extensive biological/biomedical applications. A key aspect of the proposed platform concerns the integration of magnetic levitation technology and bilateral macro–micro control system challenges. This macro–micro platform has three basic subsystems as follows: a magnetic untethered microrobotic system (MUMS), a haptic Phantom-Omni device (HPOD), and a scaled bilateral teleoperation system (SBTS). The MUMS is a magnetic propulsion-based microrobotic system, producing a biocompatible environment for the slave part of the MHMP. The MHMP uses a commercial haptic interface, HPOD, as its master side. A bilateral macro–micro teleoperation technique is employed in STBS for the telepresence of a human operator in the task environment. Such a system preserves the "feel" of the environment with which the operator interacts; Fig. 1 schematically shows the structure of the MHMP.

The MUMS shows a great deal of promise in noncontact micromanipulations [29]. The literature reports two wide categories of such systems: small magnetic gap systems (SMGS) and large magnetic gap systems (LMGS). These systems generally consist of a magnetic drive unit (MDU), which produces actuation energy for a ferromagnetic, manipulated object. In the SMGS, the manipulated object cannot be sufficiently separated from the drive unit for untethered mobile robot applications [30]–[32]. Numerous difficulties arise, however, when an attempt concerns the LMGS needed for the MUMS [33]–[35]. The MUMS has been developed from scratch at the Maglev Microrobotics Laboratory in the University of Waterloo. This system consists of two principal components: a hybrid MDU and a microrobot. The hybrid MDU has the capability to control the 3-D position and 1-D orientation controls of the microrobot. The MUMS's microrobot is basically comprised of a microgripper, electronic circuits, and a very small permanent magnet (PM). The most substantial part of the MUMS development has been focused on the design of the magnetic circuit and development of the magnetic force models. The noncontact nature of the MUMS makes it suitable for use in out-of-reach and hard-to-reach locations, such as an enclosed environment used for the biological manipulation with no risk of contamination.

A bilateral macro–micro teleoperation technology is employed to allow a human operator to feel microdomain tasks such as cell manipulation/injection and palpation. The extent of preserving the feel of an environment is characterized by the "transparency" of the system. To achieve high transparency, most of the bilateral teleoperation strategies assume that the applied force/torque from the environment can be measured by sensors directly. However, attaching force/torque sensors to our microrobot is impracticable because of the following. 1) Microscaled sensors must be attached to the microrobot for measuring forces/torques; hence, the size and weight of the floating microrobot are largely increased. 2) An on-board wireless communication device is required to access the sensors' measurements, since the microrobot is controlled without contact by the magnetic field. 3) The microscaled force/torque sensors are expensive and very sensitive to the physical parameters of an environment. An alternative approach is position-error-based (PEB) bilateral teleoperation [36], in which both the master and slave are controlled by using position measurements. The microrobot position can be measured by external laser micrometer beams with no need for contact. Considering the PEB architecture, Lawrence [37] showed that PEB with linear time-invariant controllers provides poor transparency. A gain-switching control scheme was proposed by Ni [38] to improve the transparency of PEB architecture, providing good transparency for two extreme cases: 1) the slave in free motion and 2) the slave in hard contact. In our study, the gain-switching control scheme is employed as a strategy of the SBTS for MHMP.

This paper is organized as follows. Section I has already introduced a novel platform for biomicromanipulation. Section II explains the principal of magnetic actuation, the MUMS structure description, and modeling/control of the MDU. Section III describes the concept of transparency and the gain-switching scheme. Section III presents our design for a gain-switching controller for PEB teleoperation. Section IV discusses the design of gain-switching process. Finally, Section V demonstrates the experimental evaluation and capabilities of the MHMP.

II. Principle of Magnetic Actuation and MUMS Structure

A. Principle of Magnetic Actuation

Here, the fundamental of 3-D levitated motion of a PM in an external magnetic field is reviewed. Since the PM is used as the microrobot's head, the motion control of the PM results in the control of the microrobot. Placing the PM in an external magnetic field raises the total potential energy that can be expressed as in [39]

$$U = -\int_v \mathbf{M} \cdot \mathbf{B}\, dv \tag{1}$$

where **M** is the magnetization vector of the PM, **B** is the external magnetic field vector, v is the volume of the PM, and "." denotes the dot product. Using the virtual displacement method, the unit volume magnetic force can be derived as

$$\mathbf{f} = +\nabla (\mathbf{M} \cdot \mathbf{B}). \tag{2}$$

In this study, we use a single dipole PM (it is assumed that $\mathbf{M} = [0\ 0\ M]$); therefore, the induced magnetic force due to the external magnetic field can be represented by

$$\mathbf{f} = \nabla \cdot (M\, B_z) \tag{3}$$

where B_z is the z-component of the external magnetic field **B**. For the small PM used as the head of the microrobot, the magnetization M can be taken as a constant and uniformly distributed throughout the volume. This approach simplifies the induced magnetic force on the PM as

$$\mathbf{F} = M\, (\nabla B_z)\, v. \tag{4}$$

Considering magnetic dipole moment as $dP = Mdv$, the force components applied by the external magnetic field on the PM are

$$F_x = P\frac{\partial B_z}{\partial x} \tag{5}$$

$$F_y = P\frac{\partial B_z}{\partial y} \tag{6}$$

$$F_z = P\frac{\partial B_z}{\partial z}. \tag{7}$$

Thus, the levitation force is proportional to the z-component gradients of the magnetic field. The levitation force can also be derived by Biot-Savart's law and Maxwell's equation [40], which results in the same relations as the potential energy method. Physically, inside the external magnetic field, the PM tends to move toward the minimum total potential energy location; i.e., $B_{\max}$ point—$B_{\max}$ point denotes the location of the maximum magnetic field on a horizontal plane contacting the PM. If the PM is under a steady-state condition, the gravitational force is compensated by the vertical magnetic force, and the horizontal forces equal zero, since no horizontal force exists in the $B_{\max}$ position. Hence, the position of the PM can be controlled by regulating the gradients of **B** and controlling the $B_{\max}$ location.

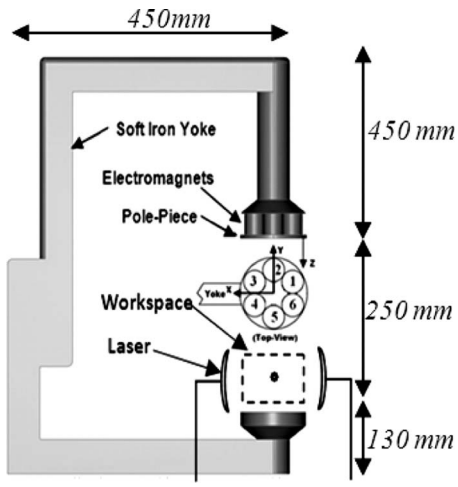

Fig. 2. Schematic of a magnetic drive unit (MDU), developed at MagLev Microrobotics Laboratory.

The torque $\boldsymbol{\tau}$ on a unit volume of the PM in the external field is $\boldsymbol{\tau} = \mathbf{M} \times \mathbf{B}$ and causes the PM to align itself with the magnetic field direction. Hence, the position and the attitude of the dipole PM can be controlled by the one-axis external magnetic field.

B. Description of MUMS

The MUMS structure consists of two main subsystems: the MDU and the microrobot. An arrangement of multiple electromagnets (six pairs) connected by a disc pole piece is employed as the MDU, shown schematically in Fig. 2. The effectiveness of this structure for 3-D motion control of the $B_{\max}$ position was reported in [7]. A soft iron yoke is used to keep the magnetic field high and uniform in the air-gap region. The relative position of the electromagnets and pole-piece geometry are two major design parameters in the determination of a working envelope for stable 3-D manipulation. The considered horizontal arrangement of electromagnets enables the MDU for the horizontal motion control of the $B_{\max}$ position. The disc pole piece has dominant functionality to configure the electromagnets' flux leakage in a way that guarantees a unique $B_{\max}$ position in the horizontal plane. The appearance of multiple $B_{\max}$ points on a horizontal plane causes unpredictability and instability of horizontal motions. Various pole pieces with different profiles were proposed and analyzed for producing the desired $B_{\max}$ [41]. The combination of finite element analysis and experiment measurements shows that a soft iron disc pole piece is capable of maintaining the unique $B_{\max}$ position inside the desired workspace. The workspace for the current setup is defined as $x,y \in$ [–10 10] mm and $z \in$ [65 95] mm. Three laser sensors for three axes are used to provide high precision displacement feedback of the microrobot for a dSPACE real-time controller. These sensors cover the working envelop of MDU with 2–8 μm resolutions.

The microrobot consists of three main components: a magnetic head, a body that includes electronic parts, and an MEMS-based microgripper. Extensive research in design and fabrication of numerous microrobots was done at the MagLev Microrobotics Laboratory. Fig. 3 presents a part of

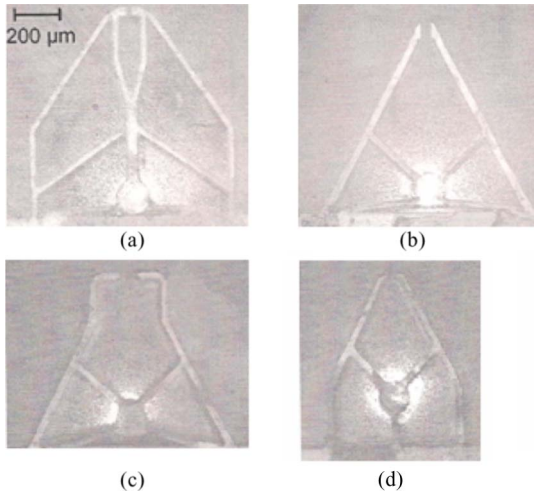

Fig. 3. Developed microgrippers for various applications of the magnetically levitated microrobot: (a) biomanipulation, (b) microsurgery, (c) microsurgery, and (d) microassembly [42].

microgrippers developed for the magnetic levitation microrobotic system [42] (the detailed design of the microrobot is not considered to be one of the key aspects of this paper and is referenced). In this paper, a simple micorobot is used to verify the performance of the proposed platform. The robot does not have a microgripper and the electronic parts, and is just a PM covered by a thin plastic body. However, more sophisticated robot equipped with various microgrippers can be used in real applications.

C. Modeling and Control of MDU

Magnetic force modeling is the first step in controlling the motion by the MDU. Since the pole piece has a considerable effect on the flux leakage of the electromagnets, the magnetic field model of electromagnets without the pole piece cannot be considered to provide a good estimation inside the workspace. Due to the circular distribution of electromagnets, loading one electromagnet and determining the magnetic field model inside the workspace allows MDU magnetic model to be derived by using the geometry transformation and superposition principle. Experimental investigations of the superposition principle showed that electromagnets interaction error in the magnetic field of MDU is less than 15%. Therefore, the superposition principle resulted in acceptable performance by simplifying the magnetic field estimation process.

The induced magnetic field of one electromagnet is measured by a gaussmeter probe. The probe was moved inside the workspace by a high precision robot while the z-component of the magnetic field was recorded. Based on the numerical analysis and experimental measurements, electromagnet number two (shown in Fig. 2) induces the following magnetic gradients:

$$\left.\frac{\partial B_z}{\partial x}\right|_{n=2} = (\alpha_x x)\, I_2 \tag{8}$$

$$\left.\frac{\partial B_z}{\partial y}\right|_{n=2} = (\alpha_y y + \beta_y)\, I_2 \tag{9}$$

$$\left.\frac{\partial B_z}{\partial z}\right|_{n=2} = (\alpha_z z + \beta_z)\, I_2 \tag{10}$$

where $\alpha_x, \alpha_y, \alpha_z, \beta_y$, and β_z and are the magnetic field parameters, determined by experimental measurement and linear least-squares curve fitting. The parameter I_2 represents the current in the electromagnet number two. By geometry transformation and the superposition principle, the unit volume magnetic force model of the system can be represented by

$$\begin{aligned}\frac{f_x}{M} = {} & \frac{x}{4}(\alpha_x + 3\alpha_y)(I_1 + I_3 + I_4 + I_6) + x\alpha_x (I_2 + I_5) \\ & + \frac{\sqrt{3}}{4} y (\alpha_x - \alpha_y)(I_1 - I_3 + I_4 - I_6) \\ & - \frac{\sqrt{3}}{2}\beta_y (I_1 - I_3 + I_6 - I_4)\end{aligned} \tag{11}$$

$$\begin{aligned}\frac{f_y}{M} = {} & \frac{y}{4}(3\alpha_x + \alpha_y)(I_1 + I_3 + I_4 + I_6) + y\alpha_y (I_2 + I_5) \\ & - \frac{\sqrt{3}}{4} x (\alpha_x - \alpha_y)(I_1 - I_3 + I_4 - I_6) \\ & + \frac{1}{2}\beta_y (I_1 + 2I_2 + I_3 - I_4 - 2I_5 - I_6)\end{aligned} \tag{12}$$

$$\frac{f_z}{M} = (\alpha_z z + \beta_z)(I_1 + I_2 + I_3 + I_4 + I_5 + I_6). \tag{13}$$

Therefore, the linearized dynamics of PM with the mass of m at the center point of the workspace $[x_c\ y_c\ z_c] = [0\ 0\ z_0]$ and $I_1 = I_2 = I_3 = I_4 = I_5 = I_6 = I_0$ can be shown as

$$m\ddot{x} - 3x(\alpha_x + \alpha_y) I_0 = -\frac{\sqrt{3}}{2}\beta_y \underbrace{(i_1 - i_3 + i_6 - i_4)}_{u_x} \tag{14}$$

$$m\ddot{y} - 3y(\alpha_x + \alpha_y) I_0 = -\frac{1}{2}\beta_y \underbrace{(i_1 + 2i_2 + i_3 - i_4 - 2i_5 - i_6)}_{u_y} \tag{15}$$

$$m\ddot{z} - \alpha_z I_0 z = (\alpha_z z_0 + \beta_z) \underbrace{(i_1 + i_2 + i_3 + i_4 + i_5 + i_6)}_{u_z} \tag{16}$$

where I_0 is the current applied to all electromagnets, and $i_j, j = 1, \ldots, 6$, is the perturbed current for the jth electromagnet. To simplify the dynamics, three virtual inputs, u_x, u_y, and u_z, are defined. u_x, u_y, and u_z are the virtual control inputs for x-axis, y-axis, and z-axis, respectively. By a control allocation matrix (CAM), virtual control inputs are mapped to the six currents for all electromagnets. Due to overactuation and coupling of the controls, it is difficult to determine an appropriate method for finding CAM. Here, the *pseudoinverse* method is used to calculate CAM. This is a constrained optimization technique that minimizes the norm of control inputs [43]. Hence, the CAM maps the virtual inputs to the electromagnets' currents with minimum energy consumption for a motion. The CAM can be

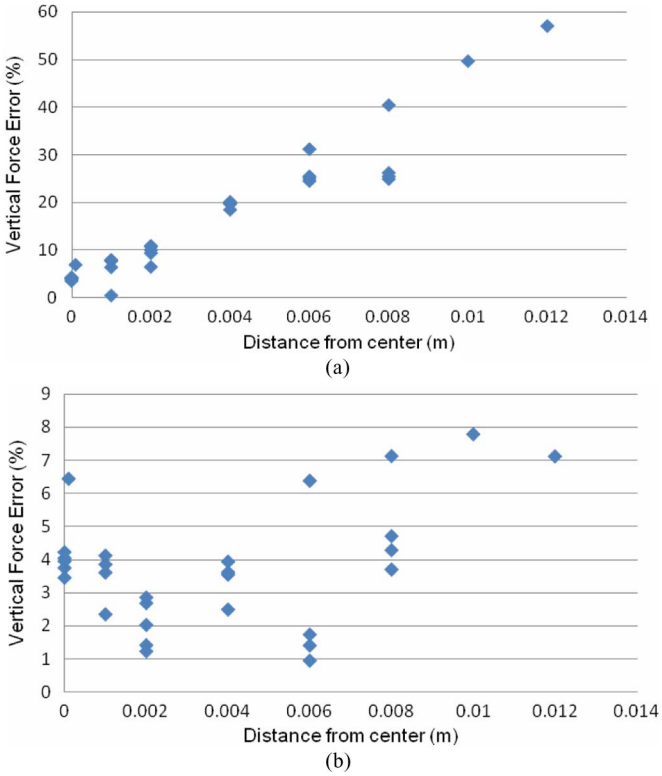

Fig. 4. (a) Magnetic force model error using the model of (13) and (b) modified magnetic force model error using the model of (18).

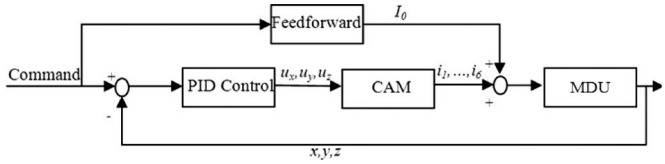

Fig. 5. Schematic diagram of the feedforward controller.

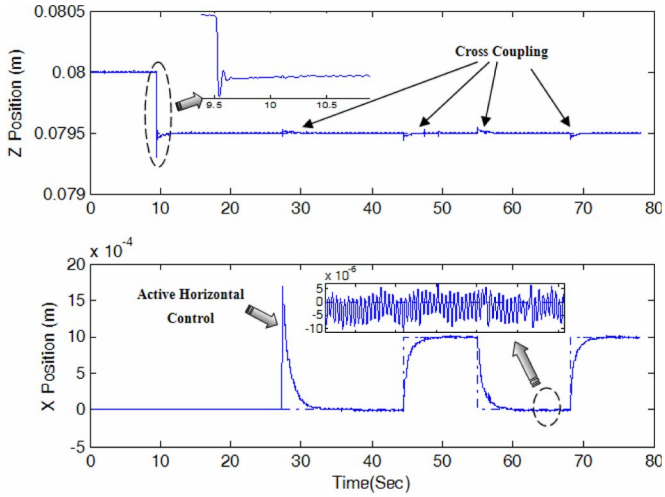

Fig. 6. Horizontal and vertical step responses.

presented as

$$\begin{bmatrix} i_1 \\ i_2 \\ i_3 \\ i_4 \\ i_5 \\ i_6 \end{bmatrix} = \underbrace{\begin{bmatrix} 0.25 & 0.08 & 0.17 \\ 0 & 0.17 & 0.17 \\ -0.25 & 0.08 & 0.17 \\ -0.25 & -0.08 & 0.17 \\ 0 & -0.17 & 0.17 \\ 0.25 & -0.08 & 0.17 \end{bmatrix}}_{\text{CAM}} \begin{bmatrix} u_x \\ u_y \\ u_z \end{bmatrix}. \tag{17}$$

The control system for the MDU was designed based on the linearized model. The experiments showed that the proposed magnetic force model in the z-direction could be modified. Since, in the z-direction, the magnetic force is equal to the weight of the levitated PM, the exact value of the magnetic force can be determined in the workspace of MDU. Therefore, the PM was randomly moved to 25 positions in the MDU workspace, and the vertical force error was calculated, as shown in Fig. 4. The modified vertical force model is represented by

$$\frac{f_z}{M} = \frac{(\alpha_z z + \beta_z)}{1 + \gamma_z d_{xy}} (I_1 + I_2 + I_3 + I_4 + I_5 + I_6) \tag{18}$$

where γ_z is a magnetic field parameter and is determined by experiment. d_{xy} is the horizontal distance of PM from the center of the MDU workspace. As in Fig. 4, increasing the distance of PM in the horizontal plane causes larger vertical force error. For the unmodified model, this error could be reached as large as 60% in the vicinity of the workspace, and for the modified model, the error is less than 9% in the MDU workspace. A feedforward-PID controller was designed based on the modified model to correct the initial linearization point, shown in Fig. 5. The feedforward signal was calculated as

$$u_{ff} = I_0 = \frac{1 + \gamma_z d_{xyc}}{M(\alpha_z z_c + \beta_z)} mg \tag{19}$$

where z_c is the command position in vertical, g is the gravity constant, and d_{xyc} is the command horizontal distance of PM from the center of workspace. The controller performance was evaluated by step response analysis in three axes, as seen in Fig. 6. The controller experimental results provide a 20-μm resolution inside the system workspace, a vertical range of 30 mm, and a horizontal range of 20 mm $\times$ 20 mm. To improve the position tracking accuracy, there are several sources of constraints, such as laser sensor resolutions, lag of amplifier, and nonuniformity of PM as the head of the microrobot. As seen in Fig. 6, there is also the cross coupling of the commands; the horizontal commands induce vertical displacement of the microrobot, which is not desirable in motion control. This cross-coupling effect acts as uncertainties in each axis of motion. The designed PID controller can handle small uncertainties such as thermal drift of electromagnets and residual magnetization of MDU, and reducing cross-coupling effect. However, advanced controller can be designed for large uncertainties such as considerable payload variation of the microrobot, planned as future work. In the following sections, a haptic interface is introduced to the system for teleoperation purposes.

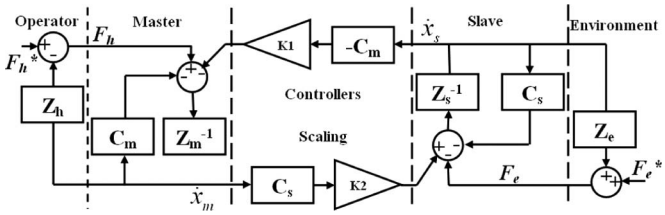

Fig. 7. Schematic of a symmetric PEB teleoperation.

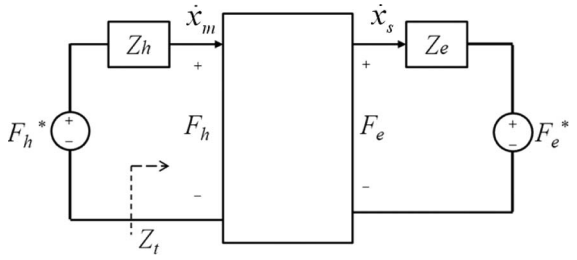

Fig. 8. Two-port model of a bilateral teleoperation.

III. Gain-Switching Control Strategy for PEB Teleoperation

In this section, the transparency analysis is first presented for a symmetric bilateral PEB system. The concept of the gain-switching scheme for transparency improvement is then reviewed based on the proposed method by Ni [38]; the stability of the gain-switching scheme in contact, free motion, and transition conditions is briefly discussed. In this study, we implemented a previously proposed PEB method; hence, the proof of theorems and lemmas are not mentioned in this paper, but can be followed in the original paper by Ni [38].

A. Transparency Analysis

A bilateral teleoperation system provides the human operator with information about the task environments. To obtain such a system, combinations of force and position measurements from the slave side can be utilized. In particular, in the PEB scheme, the reflected force to the human operator is proportional to the position error. Fig. 7 presents such a symmetric PEB system. In this figure, F_h and F_e denote hand/master and slave/environment interaction, respectively. F_h^* and F_e^* are, respectively, the operator's and environment's exogenous input forces, and both are independent of teleoperation system behavior. Generally, it is assumed that the environment and operator are passive ($F_h^* = F_e^* = 0$). The velocities of the master and slave are, respectively, defined by $\dot{x}_m$ and $\dot{x}_s$. The impedances Z_m and Z_s represent the dynamic characteristic of master and slave, respectively; both impedances include inner-loop controllers. Additionally, C_m and C_s are the impedance form of PD controllers for master and slave sides as

$$C_m(s) = K_{dm} + \frac{K_{pm}}{s} \tag{20}$$

$$C_s(s) = K_{ds} + \frac{K_{ps}}{s}. \tag{21}$$

The master and slave may have different workspaces; hence, K_1 and K_2 are the scaling factors for the mapping of workspaces. To make two workspaces overlap each other virtually, K_1 and K_2 must satisfy $K_1 \times K_2 = 1$.

To evaluate the transparency of PEB teleoperation, the two-port network model of teleoperation, shown in Fig. 8, can be represented by a hybrid impedance matrix as

$$\begin{bmatrix} F_h \\ F_e \end{bmatrix} = Z \begin{bmatrix} \dot{x}_m \\ -\dot{x}_s \end{bmatrix} \tag{22}$$

where the hybrid impedance matrix for the symmetric PEB teleoperation can be derived as

$$Z(s) = \begin{bmatrix} Z_m(s) + C_m(s) & K_2 C_m(s) \\ K_1 C_s(s) & Z_s(s) + C_s(s) \end{bmatrix}. \tag{23}$$

Perfect transparency [37] is achieved with and only with a perfect match of the environment impedance $Z_e = F_e/\dot{x}_s$ to the impedance transmitted to the operator's hand $Z_h = F_h/\dot{x}_m$. In practice, a perfectly transparent teleoperation will not be possible with PEB architecture, so it makes sense to investigate the transparency in specific cases: a slave in free motion ($Z_e \to 0$) and a slave in hard contact ($Z_e \to \infty$). For the PEB architecture, the transmitted impedance to the operator's hand can be obtained from the hybrid impedance matrix as

$$Z_h = Z_m + C_m - \frac{C_m C_s}{Z_e + Z_s + C_s} \tag{24}$$

when the slave in free motion, $Z_e \to 0$; Z_h becomes

$$Z_h = Z_m + \frac{C_m Z_s}{Z_s + C_s}. \tag{25}$$

Achieving complete transparency in free motion requires $Z_h \to 0$. Since all the impedances have positive values, the transmitted impedance cannot be zero ($Z_h > Z_m$). If the master PD controller has very low gains and the slave PD controller has very high gains, the impedance of the master is transmitted to the operator's hand. Furthermore, the high gain of the slave PD controller causes good position tracking in free motion. When the slave in hard contact, $Z_e \to \infty$; Z_h becomes

$$Z_h \to Z_m + C_m. \tag{26}$$

This equation represents that the dynamics of the master and its controller is transmitted to the operator's hand. However, if the master controller has very high gain and the slave controller has very low gain, the feel of hard contact can be transmitted to the operator's hand by high impedance. In addition, the low gain of slave PD controller avoids hard collision with the hard contact. Therefore, a gain-switching control scheme will enhance transparency of the PEB teleoperation in free motion and hard contact cases.

B. Stability of Teleoperation

The stability of a teleoperation system depends on the human operator knowledge and environment dynamics. Human operator dynamics is highly adaptive, and the environment impedance is also usually unknown. Therefore, it is necessary to find stability conditions, absolute stability, which depends only on the

teleoperator. Based on Llewellyn's criteria, the PEB teleoperation system is absolutely stable if all the gains of master and slave PD controllers are positive and $K_{pm}/K_{ps} = K_{dm}/K_{ds}$, Theorem 1 in [38]. Therefore, the absolute stability only depends on the controller gains. It does not require any parameters of the master or slave dynamics, which usually contain modeling uncertainty. However, the condition given by Llewellyn's criteria guarantees absolute stability only of a liner time-invariant system. In our case, this dynamics applies when the teleoperation system is well inside either the free motion or hard contact. However, the dynamics of the system is time varying in the contact transition.

During the contact transition, the system dynamics is switching between unconstrained space and constrained space. Physically, the slave manipulator is kicked back by the contact surface for a few times, a situation called transition mode. Absolute stability is necessary, but not a sufficient condition for teleoperation stability. Ni [38] investigated the asymptotic stability of the PEB teleoperation system in a constrained space, unconstrained space, and transition mode. The gain switching to achieve better transparency makes the contact transition stability more complicated.

To investigate the absolute stability of gain switching, two sets of controllers are presented. The PD controller gains for free motion are defined as $\{K_{pm}^{l}, K_{dm}^{l}, K_{ps}^{h}, K_{ds}^{h}\}$ and for hard contact as $\{K_{pm}^{h}, K_{dm}^{h}, K_{ps}^{l}, K_{ds}^{l}\}$. Ni [38] showed the asymptotic stability of asynchronous gain switching in the following cases: unconstrained motion with unconstrained gains, constrained motion with unconstrained gains, unconstrained motion with constrained gains, and constrained motion with constrained gains [38].

IV. Design of the Gain-Switching Controller for the MHMP

Based on the transparency analysis in the previous section, the gain switching should be applied for the master and the slave PD controllers. In this section, we first present the gain-switching rules, and tuning process of experimental parameters. The experimental setup is then illustrated for the MHMP.

A. Design of Gain-Switching Rules

Achieving transparency requires the gain switching between high and low for master and slave controllers. Since two extreme cases, free motion and hard contact, are considered in this study, the gain switching can be triggered by the filtered position error δ of the system as

$$\delta = \left\| k_p e + k_i \int e \, dt \right\| \tag{27}$$

where e is the position error, the difference between the scaled position of the master and the real position of the slave. Two parameters k_p and k_i were determined by experiments. The parameter δ was measured in both free motion and contact cases, and then two parameters δ_{free} and $\delta_{\mathrm{contact}}$ were tuned for the following gain-switching rules:

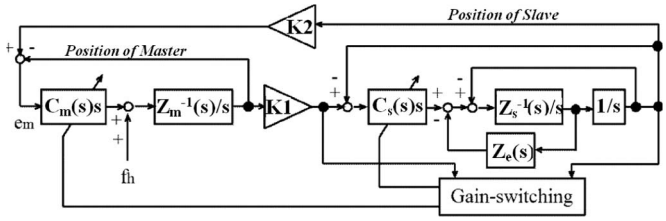

Fig. 9. Block diagram of a gain-switching control scheme.

1) if the master PD controller is low and the slave PD controller is high and $\delta > \delta_{\mathrm{contact}}$, then the master should be switched to high and the slave to low;
2) if the master PD controller is high and the slave PD controller is low and $\delta < \delta_{\mathrm{free}}$, then the master should be switched to low and the slave to high; and
3) otherwise the controller gains are not switched.

Fig. 9 presents the block diagram of the gain-switching teleoperation system. All the switching parameters, $\gamma = [k_p, k_i, \delta_{\mathrm{free}}$ and $\delta_{\mathrm{contact}}]$, were tuned experimentally and changing any of them can change the sensitivity of switching.

B. Tuning the Gain-Switching Parameters

Finding proper gain-switching parameters, γ, influences the MHMP performance. Hence, a considerable experimental analysis is required to tune these parameters. The position errors are first recorded for a series of random motions inside the workspace, with no presence of hard contact. Therefore, a bound of the filtered position errors can be determined for the free motion tasks. The parameter δ_{free} can then be selected as the upper range of the filtered position errors. Choosing the parameter $\delta_{\mathrm{contact}}$ significantly depends on the sensitivity of task. Generally, this parameter is larger than δ_{free}. For slow and very sensitive tasks, $\delta_{\mathrm{contact}}$ is selected close to the δ_{free} to reduce the risk of damage for the manipulated object, but if these two parameters are selected very close to each other, that possibly causes undesirable high-frequency switching in contact transition mode. To avoid switching, a relatively larger value is selected for $\delta_{\mathrm{contact}}$, so the sensitivity in encountering hard contact is reduced.

Choosing suitable k_p and k_i can compensate for the sensitivity of contact detection if a large $\delta_{\mathrm{contact}}$ is used. If the integral part of the filtered error has a larger value relative to the proportional part, by increasing the gain k_i, the gain switching provides an acceptable switching time in contact detection. Therefore, based on the tasks, there is a tradeoff for selecting the gain-switching parameters. In our study, several sets of gain-switching parameters of different sensitivities were considered. The following section discusses experimental analysis of the MHMP.

C. Experimental Setup

The experimental setup, as shown in Fig. 10, consists of a Phantom Omni device as the master and the MUMS as the slave. SensAble Technologies Phantom Omni is a force feedback haptic device, and it is often used in many pieces of research in haptic and telerobotic [44], [45]. The nominal resolution for

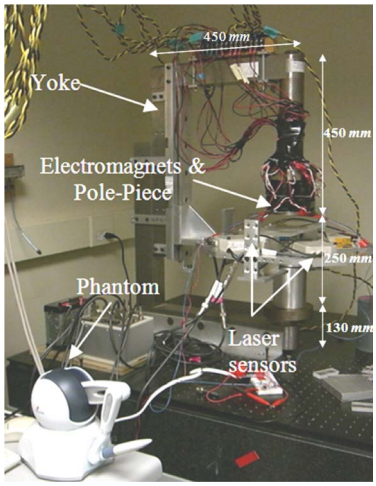

Fig. 10. Experimental setup of the MHMP.

this device is 0.55 mm and can cover the motion range of hand movement pivoting at wrist. The maximum exertable force at its nominal position is 3.3 N. The Phantom is connected to a Linux computer by a Firewire IEEE1394 port. The master site communicates with the slave site via Ethernet. The UDP/IP was implemented, since it can communicate faster than TCP/IP. The master site can communicate with the slave site via both Ethernet and optical fiber.

The slave site includes the MUMS and dSPACE real-time controller connected to a windows computer. The slave site has three position inputs and three forces as outputs. The position controls received by a windows computer over UDP/IP from a Linux computer are sent to dSPACE controller with optical fiber connection. The controller produces the current for the electromagnets of the MUMS based on the position commands from the master site. The controllers also compute the three forces for haptic application and send them to the master site; the system data flow is schematically shown in Fig. 1.

V. Experimental Evaluation

The proposed MHMP was tested on the experimental setup described in Sections II and III. The microrobot used in this experiment consists of one cylindrical neodymium magnet and the outer body made of plastic. The plastic body is used to protect the magnets from damaging and allow a larger range for the horizontal motion. The size of microrobot is 10 mm $\times$ 10 mm $\times$ 5 mm and its mass is 0.01 kg. To have stiff environment (hard contact) in the experiment, a sheet of plexiglass was used. The lasers detect microrobot through plexiglass.

The switching parameters $\gamma = [k_p, k_i, \delta_{\text{free}}$, and $\delta_{\text{contact}}]$ are selected by trial-and-error as $\gamma = [0.9, 0.1, 0.0007$, and $0.001]$. δ_{free} and δ_{contact} should be selected to make asynchronous switching [38]. The gain switching is defined as, when the gain switch to 1, the PD controllers gains are $K^h_{pm} = 200$, $K^h_{dm} = 2$, $K^l_{ps} = 0.2$, $K^1_{ds} = 0.002$ and when the gain switch to 0, the PD controller gains are $K^l_{pm} = 0.1$, $K^l_{dm} = 0.001$, $K^h_{ps} = 1$, $K^h_{ds} = 0.01$. The superscripts l and h denote low and high, respectively. The gains are tuned by trial and error, subject to the stability conditions $K^h_{pm}/K^l_{ps} = K^h_{dm}/K^l_{ds}$, $K^l_{pm}/K^h_{ps} = K^l_{dm}/K^h_{ds}$.

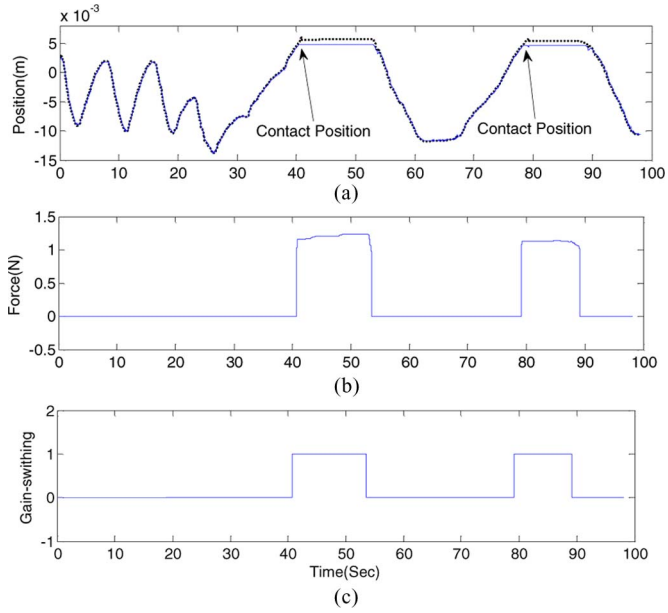

Fig. 11. Experimental results of a gain-switching control in z-direction motions: (a) scaled master position (. . .) and slave position (—), (b) haptic force, and (c) gain-switching.

The experimental results were shown in Fig. 11. This figure shows the vertical motion of the microrobot relative to the center of the workspace. The phantom motion is in the range $[-40\ 40]$ mm and mapped to $[-65\ 95]$ mm as the microrobot motion range. A hard contact was placed in the z-direction at 4.72 mm from the center of workspace. The switching occurred with 150 ms delay, which is acceptable for this application. Fig. 12 presents the teleoperation position tracking error; it shows that the rms of tracking error in free motion is 40 μm. In a small range of motion, the laser sensor can provide ultrahigh accuracy position feedbacks. Hence, several experiments have been investigated in a small range to enhance the motion resolutions. Fig. 13 presents the teleoperation performance in controlling the microrobot performance in free motions. In the motion range of 2 mm at center of laser workspace, the rms of the position tracking error is 20 μm.

In another set of experiment, the microrobot is moved in unknown viscous liquid. Since the dynamics of an environment is not considered in the design process, the rms of position tracking error becomes as large as 30 μm, shown in Fig. 14. This experiment shows a promising capability of the MHMP in maintaining the system's accuracy in various unknown environments. The human operator can plan a micromanipulation task in a way that a degraded manipulation can be accomplished. For example, the human operator can feel roughly the environment's physical properties by comparing the slave and master positions. The human operator can modify the trajectory of slave-microrobot for a micromanipulation task based on observations in various accomplished experiments. Hence, this investigation presents performance robustness and the importance of haptic

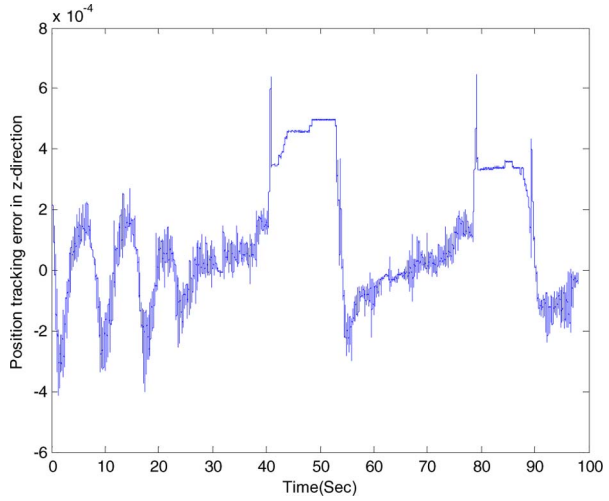

Fig. 12 Position tracking error in z-direction motion with wide range of operation.

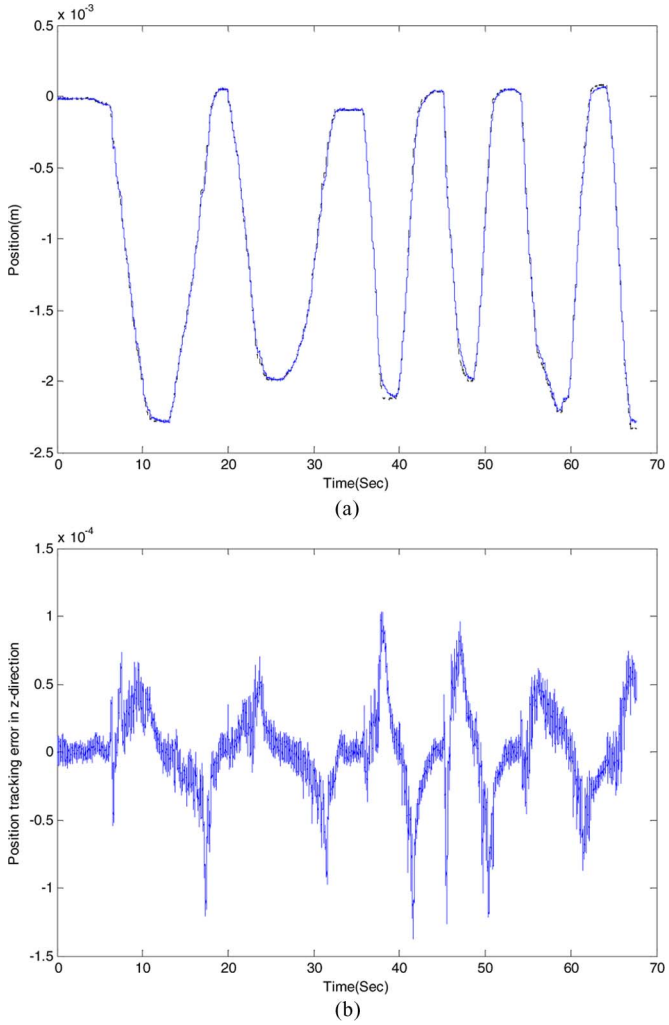

Fig. 13. Free motion of a microrobot in small range task: (a) scaled master position (. . .) and slave position and (b) tracking error in the z-direction.

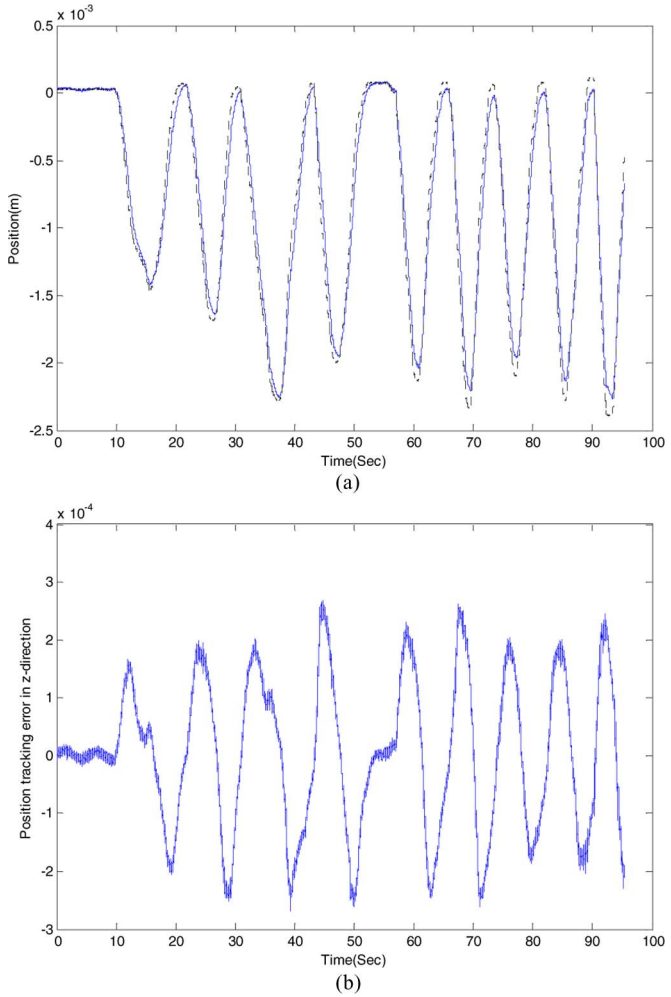

Fig. 14. Free motion of a microrobot in small range task in a viscous fluid: (a) scaled master position (. . .) and slave position and (b) tracking error in the z-direction.

application, where the human operator intends to manipulate object with no knowledge of environment's physical properties.

VI. Conclusion

In this paper, a novel MHMP was proposed. The device consists of three basic subsystems: micro magnetically levitated slave robot, macro master robot, and scaled bilateral teleoperation system. The developed magnetic propulsion-based system and Phantom Omni device were used as the micro slave robot and the haptic master robot, respectively. SBTS was expected to enable a human operator to control the micro slave robot by manoeuvring the macro master haptic robot. A previously developed gain-switching scheme was used to achieve transparent PEB teleoperation. The performance of a system was investigated in two extreme cases. From several experimental results, it was confirmed that when the slave was in free motion, the slave tracked the scaled trajectory of the master with rms of tracking error 20–40 μm in free motions, and when the slave was in a contact with an object, an operator could perceive it and keep the contact situation. The robustness of a platform in

unknown environments has been investigated in various manipulation tasks. The levitated microrobot can be remotely manipulated in a 20 mm × 20 mm × 30 mm workspace.

REFERENCES

[1] F. Arai, H. Maruyama, T. Sakami, A. Ichikawa, and T. Fukuda, "Pinpoint injection of microtools for minimally invasive micromanipulation of microbe by laser trap," *IEEE/ASME Trans. Mechatronics*, vol. 8, no. 1, pp. 3–9, Mar. 2003.

[2] C. Pawashe, S. Floyd, and M. Sitti, "Multiple magnetic microrobot control using electrostatic anchoring," *Appl. Phys. Lett.*, vol. 94, p. 164108, Apr. 2009.

[3] P. K. Wong, T.-H. Wang, J. H. Deval, and C.-M. Ho, "Electrokinetics in micro devices for biotechnology applications," *IEEE/ASME Trans. Mechatronics*, vol. 9, no. 2, pp. 366–376, Jun. 2004.

[4] P. Basset, A. Kaiser, B. Legrand, D. Collard, and L. Buchaillot, "Complete system for wireless powering and remote control of electrostatic actuators by inductive coupling," *IEEE/ASME Trans. Mechatronics*, vol. 12, no. 1, pp. 23–31, Feb. 2007.

[5] Z. Zhang, K. Huang, and C.-H. Menq, "Design, implementation, and force modeling of quadrupole magnetic tweezers," *IEEE/ASME Trans. Mechatronics*, vol. 15, no. 5, pp. 704–713, Oct. 2010.

[6] H. Zhang, E. Burdet, A. N. Poo, and D. W. Hutmacher, "Microassembly fabrication of tissue engineering scaffolds with customized design," *IEEE Trans. Autom. Sci. Eng.*, vol. 5, no. 3, pp. 446–456, Jul. 2008.

[7] M. Savia and H. N. Koivo, "Contact micromanipulation—Survey of strategies," *IEEE/ASME Trans. Mechatronics*, vol. 14, no. 4, pp. 504–514, Aug. 2009.

[8] Y. Zhang, B. K. Chen, X. Liu, and Y. Sun, "Autonomous robotic pick-and-place of microobjects," *IEEE Trans. Robot.*, vol. 26, no. 1, pp. 200–207, Feb. 2010.

[9] M. Rakotondrabe, Y. Haddab, and P. Lutz, "Development, modeling, and control of a micro-/nanopositioning 2-DOF stick–slip device," *IEEE/ASME Trans. Mechatronics*, vol. 14, no. 6, pp. 733–745, Dec. 2009.

[10] C.-C. Lan, C.-M. Lin, and C.-H. Fan, "A self-sensing microgripper module with wide handling ranges," *IEEE/ASME Trans. Mechatronics*, vol. 16, no. 1, pp. 1–10, Feb. 2011.

[11] Y. Zhang, M. Cong, D. Guo, and D. Wang, "Design optimization of a bidirectional microswimming robot using giant magnetostrictive thin films," *IEEE/ASME Trans. Mechatronics*, vol. 14, no. 4, pp. 493–503, Aug. 2009.

[12] B. Kim, S. Park, and J.-O. Park, "Microrobots for a capsule endoscope," in *Proc. IEEE/ASME Int. Conf. Adv. Intell. Mechatronics (AIM)*, 2009, pp. 729–734.

[13] M. Simi, P. Valdastri, C. Quaglia, A. Menciassi, and P. Dario, "Design, fabrication, and testing of a capsule with hybrid locomotion for gastrointestinal tract exploration," *IEEE/ASME Trans. Mechatronics*, vol. 15, no. 2, pp. 170–180, Apr. 2010.

[14] F. van Breugel, W. Regan, and H. Lipson, "From insects to machines," *IEEE Robot. Autom. Mag.*, vol. 15, no. 4, pp. 68–74, Dec. 2008.

[15] B. R. Donald, C. G. Levey, C. D. McGray, I. Paprotny, and D. Rus, "An untethered, electrostatic, globally controllable MEMS micro-robot," *J. Microelectromech. Syst.*, vol. 15, pp. 1–15, 2006.

[16] C. Elbuken, L. Gui, C. L. Ren, M. Yavuz, and M. B. Khamesee, "Design and analysis of a polymeric photo-thermal microactuator," *Sensors Actuators A: Phys.*, vol. 147, pp. 292–299, 2008.

[17] C. Elbuken, M. B. Khamesee, and M. Yavuz, "Design and implementation of a micromanipulation system using a magnetically levitated MEMS robot," *IEEE/ASME Trans. Mechatronics*, vol. 14, no. 4, pp. 434–445, Aug. 2009.

[18] M. T. Hou, H. Shen, and G. Jiang, "A rolling locomotion method for untethered magnetic microrobots," *Appl. Phys. Lett.*, vol. 96, pp. 024102-1–024102-3, Jan. 2010.

[19] R. Spero, L. Vicci, J. Cribb, D. Bober, V. Swaminathan, E. O'Brien, S. Rogers, and R. Superfine, "High throughput system for magnetic manipulation of cells, polymers, and biomaterials," *Rev. Sci. Instrum.*, vol. 79, p. 083707, 2008.

[20] G. R. Souza, J. R. Molina, R. M. Raphael, M. G. Ozawa, D. J. Stark, C. S. Levin, L. F. Bronk, J. S. Ananta, J. Mandelin, M. Georgescu, J. A. Bankson, J. G. Gelovani, T. C. Killian, W. Arap, and R. Pasqualini, "Three-dimensional tissue culture based on magnetic cell levitation," *Nat. Nano*, vol. 5, pp. 291–296, 2010.

[21] N. Ando, P. Korondi, and H. Hashimoto, "Networked telemicromanipulation systems "Haptic loupe"," *IEEE Trans. Ind. Electron.*, vol. 51, no. 6, pp. 1259–1271, Dec. 2004.

[22] K. Vlachos and E. Papadopoulos, "Analysis and experiments of a haptic telemanipulation environment for a microrobot driven by centripetal forces," *J. Comput. Inf. Sci. Eng.*, vol. 8, pp. 041007-1–041007-9, 2008.

[23] P. Estevez, S. Khan, P. Lambert, M. Porta, I. Polat, C. Scherer, M. Tichem, U. Staufer, H. Langen, and R. Schmidt, "A Haptic Tele-operated System for Microassembly," *Precision Assem. Technol. Syst.*, vol. 315, pp. 13–20, 2010.

[24] S. Khan and A. Sabanovic, "Force feedback pushing scheme for micromanipulation applications," *J. Micro-Nano-Mechatronics*, vol. 5, pp. 43–55, 2009.

[25] B. T. Bethea, A. M. Okamura, M. Kitagawa, T. P. Fitton, S. M. Cattaneo, V. L. Gott, W. A. Baumgartner, and D. D. Yuh, "Application of haptic feedback to robotic surgery," *J. Laparoendoscopic Adv. Surgical Tech.-Part A*, vol. 14, no. 3, pp. 191–195, 2004.

[26] A. Talasaz, R. V. Patel, and M. D. Naish, "Haptics-enabled teleoperation for robot-assisted tumor localization," in *Proc IEEE Int. Conf. Robot. Autom. (ICRA), 2010*, pp. 5340–5345.

[27] A. Sieber, P. Valdastri, K. Houston, C. Eder, O. Tonet, A. Menciassi, and P. Dario, "A novel haptic platform for real time bilateral biomanipulation with a MEMS sensor for triaxial force feedback," *Sensors Actuators A, Phys.*, vol. 142, p. 19, 2008.

[28] M. Zareinejad, S. M. Rezaei, A. Abdullah, and S. S. Ghidary, "Development of a piezo-actuated micro-teleoperation system for cell manipulation," *Int. J. Med. Robot. Comput. Assisted Surgery*, vol. 5, pp. 66–76, 2009.

[29] D. Craig and M. B. Khamesee, "Motion control of a large gap magnetic suspension system for microrobotic manipulation," *J. Phys. D*, vol. 40, p. 3277, 2007.

[30] C. Fulford, M. Maggiore, and J. Apkarian, "Control of a 5 DOF magnetically levitated positioning stage," *IEEE Trans. Control Syst. Technol.*, vol. 17, no. 4, pp. 844–852, Jul. 2009.

[31] Z. Zhang and C. Menq, "Six-axis magnetic levitation and motion control," *IEEE Trans. Robot.*, vol. 23, no. 2, pp. 196–205, Apr. 2007.

[32] W. Kim and S. Verma, "Multiaxis maglev positioner with nanometer resolution over extended travel range," *J. Dyn. Sys., Meas., Control*, vol. 129, pp. 777–785, Nov. 2007.

[33] J.-B. Mathieu, G. Beaudoin, and S. Martel, "Method of propulsion of a ferromagnetic core in the cardiovascular system through magnetic gradients generated by an MRI system," *IEEE Trans. Biomed. Eng.*, vol. 53, no. 2, pp. 292–299, Feb. 2006.

[34] S. Tamaz, R. Gourdeau, A. Chanu, J.-B. Mathieu, and S. Martel, "Real-time MRI-based control of a ferromagnetic core for endovascular navigation," *IEEE Trans. Biomed. Eng.*, vol. 55, no. 7, pp. 1854–1863, Jul. 2008.

[35] T. Ohji, H. Hara, K. Amei, and M. Sakui, "Three-dimensional motion of a small object by using a new magnetic levitation system having four I-shaped electromagnets," *IEEE Trans. Magn.*, vol. 44, no. 11, pp. 4159–4162, Nov. 2008.

[36] G. J. Raju, G. C. Verghese, and T. B. Sheridan, "Design issues in 2-port network models of bilateral remote manipulation," in *Proc. Robot. Autom.*, 1989, vol. 3, pp. 1316–1321.

[37] D. A. Lawrence, "Stability and transparency in bilateral teleoperation," *IEEE Trans. Robot. Autom.*, vol. 9, no. 5, pp. 624–637, Oct. 1993.

[38] L. Ni and D. W. L. Wang, "A gain-switching control scheme for position-error-based bilateral teleoperation: Contact stability analysis and controller design," *Int. J. Robot. Res.*, vol. 23, pp. 255–274, Mar. 2001.

[39] J. A. Stratton, *Electromagnetic Theory*. Hoboken, NJ: Wiley, 2007.

[40] M. B. Khamesee, N. Kato, Y. Nomura, and T. Nakamura, "Design and control of a microrobotic system using magnetic levitation," *IEEE/ASME Trans. Mechatronics*, vol. 7, no. 1, pp. 1–14, Mar. 2002.

[41] M. B. Khamesee and E. Shameli, "Pole piece effect on improvement of magnetic controllability for noncontact micromanipulation," *IEEE/ASME Trans. Magn.*, vol. 43, no. 2, pp. 533–542, Feb. 2007.

[42] C. Elbuken, "Magnetic levitation of polymeric photo-thermal microgrippers," Ph.D. dissertation, Dept. Mech. Eng., Univ. of Waterloo, Waterloo, ON, 2008.

[43] M. W. Oppenheimer, D. B. Doman, and M. A. Bolender, "Control allocation for over-actuated systems," in *Proc. 14th Mediterranean Conf. Control Autom. (MED '06)*, pp. 1–6.

[44] M. Tavakoli, R. V. PateI, and M. Moallem, "Design issues in a haptics-based master-slave system forminimally invasive surgery," in *Proc. IEEE Int. Conf. Robot. Autom. (ICRA)*, 2004, vol. 1, pp. 371–376.

[45] F. Mobasser and K. Hashtrudi-Zaad, "Implementation of a rate mode impedance reflecting teleoperation controller on a haptic simulation system," in *Proc. IEEE Int. Conf. Robot. Autom. (ICRA)*, 2004, vol. 2, pp. 1974–1979.

Moein Mehrtash (M'10) received the B.Sc. and M.Sc. degrees in flight dynamics and control from Sharif University of technology, Tehran, Iran. He is currently working toward the Ph.D. degree in the MagLev Microrobotics Laboratory, University of Waterloo, Waterloo, ON, Canada.

His research interests include control system design, haptic teleoperation, and magnetic drive technology.

Naoaki Tsuda received the B.E. and M.E. degrees in mechanical engineering in 1999 and 2001, respectively, and the D.E. degree in system engineering in 2004, all from Mie University, Tsu City, Japan.

Since 2005, he has been an Assistant Professor in the Department of Mechanical Engineering, Wakayama National College of Technology, Gobo, Japan. From 2010 to 2011, he is a Visiting Scholar collaborating with Dr. Khamesee in the Department of Mechanical and Mechatronics Engineering, University of Waterloo, Waterloo, ON, Canada. His research interests include human interface, welfare mechatronics, and magnetic levitation.

Dr. Tsuda is a member of the Japan Society of Mechanical Engineers, the Robotics Society of Japan, and the Human Interface Society (Japan).

Mir Behrad Khamesee (M'04) received the M.S. and Ph.D. degrees from Mie University, Tsu City, Japan in 1996 and 1999, respectively, both in mechanical engineering (mechatronics) and under a Japanese government scholarship.

He worked in industry in Japan from 1999 to 2002. He held a Postdoctoral position at the University of Alberta, Edmonton, AB, Canada, from 2002 to 2003. In March 2004, he was appointed as an Assistant Professor at the University of Waterloo, Waterloo, ON, Canada, and in July 2009, he was promoted to Associate Professor. His research interests and expertise include design, modeling, and control of advanced mechatronics systems, particularly microrobotic magnetic levitation and electromagnetic dampers. He is the Director of the MagLev Microrobotics Laboratory, University of Waterloo, Waterloo, ON, Canada.

Dr. Khamesee is involved in conferences program committees, has organized several sessions at international conferences, and is a technical reviewer for several IEEE journals.